Astron. & Astrophys. 37, 81 – 86 (1974)

The Thermal Emission of the Dust Corona, during the Eclipse of June 30, 1973

II. Photometric and Spectral Observations

P. Léna* and Y. Viala**
Université Paris VII et Observatoire de Meudon

D. Hall
Kitt Peak National Observatory***

A. Soufflot
Laboratoire de Physique Stellaire et Planétaire

Received August 22, 1974

Summary. Observations of the F-corona have been made in the 10 μ region of the infrared during the eclipse of June 30, 1973. Use of the supersonic aircraft "Concorde 001" permitted 74 min of observation during totality and greatly reduced problems due to sky noise. The plane of the ecliptic was scanned over heliocentric distances of from 3 to 19 solar radii off the east limb. Bright features previously observed at shorter wavelengths, notably emission at 4 solar radii are evident on the 10 μ scans, strongly indicating that the radiation is due to thermal emission by dust. The specific intensity in the 4 $R_\odot$ feature is 5 μW cm^{-2} sterad^{-1} μ^{-1} higher than the intensity 22 arcmin above the ecliptic. Spectra were taken at one region in the ecliptic and tentatively attributed to silicate-type material.

Key words: F-corona — interplanetary dust — eclipse

Introduction

Observations of near infrared (1–5 μ) emission by the F-corona and their theoretical interpretation have advanced markedly since the early work of Peterson (1963, 1967), Harwit (1964) and MacQueen (1968). The existence of areas of increased brightness in the plane of the ecliptic, the most prominent occurring 4 solar radii ($R_\odot$) from the sun's center, is now well established (Peterson, 1967, 1971; MacQueen, 1968; Koutchmy, 1972). The quantitative theory of their origin in thermal emission by hot dust has been developed (Kaiser, 1970; Lamy, 1974) although this interpretation is not universally accepted (Calbert and Beard, 1972).

As originally pointed out by MacQueen (1968), longer wavelength infrared observations of the F-corona should permit a definitive assessment of the relative contributions of scattering and emission effects to the total radiation. Further, as many potential dust components have characteristic spectra in the 10 and 20 μ regions, spectral observations should yield useful information as to the actual composition of the dust. An attempt to obtain such observations was made during the eclipse of 7 March, 1970 in Mexico (Mankin *et al.*, 1974). Unfortunately sky noise made spectral observations impractical and severely limited the sensitivity of photometric observations.

The present paper describes observations obtained in a similar experiment flown on the supersonic aircraft "Concorde 001" during the June 30, 1973 eclipse over West Africa. The flight and experiments have been summarized in a general paper (Beckman *et al.*, 1973) and the instrumentation used in the infrared F-coronal experiment is described in an earlier paper (Léna *et al.*, 1974). The objectives of the experiment were to map the spatial distribution of F-coronal brightness around the plane of the ecliptic in three wavelength intervals (1.8–2.4 μ, 3.6–4.8 μ and 8–13 μ) and to obtain moderate resolution ($\lambda/\Delta\lambda \sim 30$–50) spectra of bright features. Unfortunately the 4 μ channel did not yield useful data due to detector contamination which reduced sensitivity. The 2 μ channel operated satisfactorily but the data was not recorded due to a fault in the multiplexer and analog to digital converter. The 10 μ system performed

* "Equipe de Recherche associée au CNRS—Astronomie Infrarouge".
** On leave at Institut für Astrophysik, Bonn, RFA.
*** Operated by the Association of Universities for Research in Astronomy, Inc., under contract with the National Science Foundation.

as planned and the results obtained are presented in the following sections.

During the same eclipse, ground observations were made at 2.2 μ by Koutchmy and Lamy and may be compared to the 10 μ results (Lamy and Koutchmy, 1974).

Photometric Observations

The first 50 min of the 74 min totality were devoted to the mapping of the spatial distribution of the coronal brightness in an 8–13 μ bandpass. The chopped apertures in the focal plane (Léna *et al.*, 1974) were aligned perpendicular to the ecliptic so that the modulated signal represented the brightness difference between a circular area of 4.2′ diameter in the ecliptic and another 22′ below it. This arrangement has the advantage of cancelling circularly symmetric radiation and, on the basis of MacQueen's (1968) mapping, the modulated signal should measure excess brightness in the plane of the ecliptic.

Ten radial scans were made to the east nearly along the ecliptic and close to the invariable plane of the solar system by scanning the gyroheliostat, the distance from the sun's center varying from 3 $R_\odot$ up to 19 $R_\odot$. The parameters of individual scans are summarized in Table 1 and their configuration with respect to the sun and the ecliptic is shown in Fig. 1. The heliocentric distance scale was established by observation of the eclipsed sun relative to a calibrated scale and is subject to errors of the order of $\pm 3'$. Five of the scans have been discarded for various reasons. Problems with the voice recording channel prevent determination of a positive distance scale for Scan *A*. Rotation of the field due to the motion of the aircraft during totality was not entirely nulled by compensation rates fed into the gyro

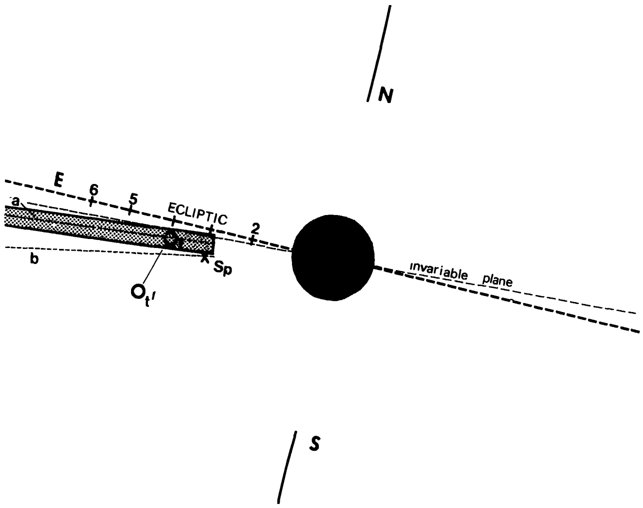

Fig. 1. Configuration of the scans in the focal plane. Grey area shows the position of the center of the main diaphragm (t) for Scans *A* to *F*, parallel to axis (a). Scans *G* to *K* were shifted toward axis (b). Respective positions of diaphragms t and t′ are shown, their assembly moving parallel to the scanning axis. The cross Sp marks the position where spectra are taken

and Scans *G*, *H*, *I* and *J* are not close enough to the ecliptic to include regions of enhanced brightness. They do not, in fact, show the structure apparent on the Scans *B*, *C*, *D*, *E* and *F* which are in the ecliptic (and have reliable heliocentric distance scales), although they have the same general slope outward from the Sun.

The acceptable Scans *B–F*, are shown in Fig. 2. The intensity calibration of these is discussed in a later section. The zero (balance between the two apertures) was set just prior to second contact but drifted slightly during totality due to changes in temperature in the apparatus (particularly the window). The drift was very

Table 1. Description of the observing sequence

Name	Time	Approximate scan extension ($R_\odot$)	Duration (s)	Mode	Scan direction	Comment
—	$10^{h}53^{m}$	second contact				
A	$10^{h}56^{m}19^{s}$	3 to 7	64	wideband	(a)	bad acquisition
B	$10^{h}58^{m}32^{s}$	3 to 9	96	wideband	(a)	good-slight DC offset
C	$11^{h}00^{m}37^{s}$	3 to 10	102	wideband	(a)	good
D	$11^{h}03^{m}13^{s}$	3 to 9	96	wideband	(a)	good
E	$11^{h}05^{m}02^{s}$	3 to 15	192	wideband	(a)	good
F	$11^{h}10^{m}49^{s}$	3 to 10	112	wideband	(a)	good-slight DC offset
Z	$11^{h}13^{m}$	tangential, 5′	120	wideband	⊥(a)	good; but scanning speed too low
G	$11^{h}18^{m}02^{s}$	3 to 10	112	wideband	(b)	mediocre, moves toward (b),
H	$11^{h}24^{m}18^{s}$	3 to 14	160	wideband	(b)	mediocre, moves toward (b),
I	$11^{h}31^{m}03^{s}$	2 to 17	240	wideband	(b)	mediocre, moves toward (b),
K	$11^{h}40^{m}00^{s}$	3 to 12	144	wideband	(b)	mediocre, moves toward (b),
S	$11^{h}45^{m}20^{s}$	3	384	spectrum	—	good
—	$12^{h}03^{m}$		end of measurements			

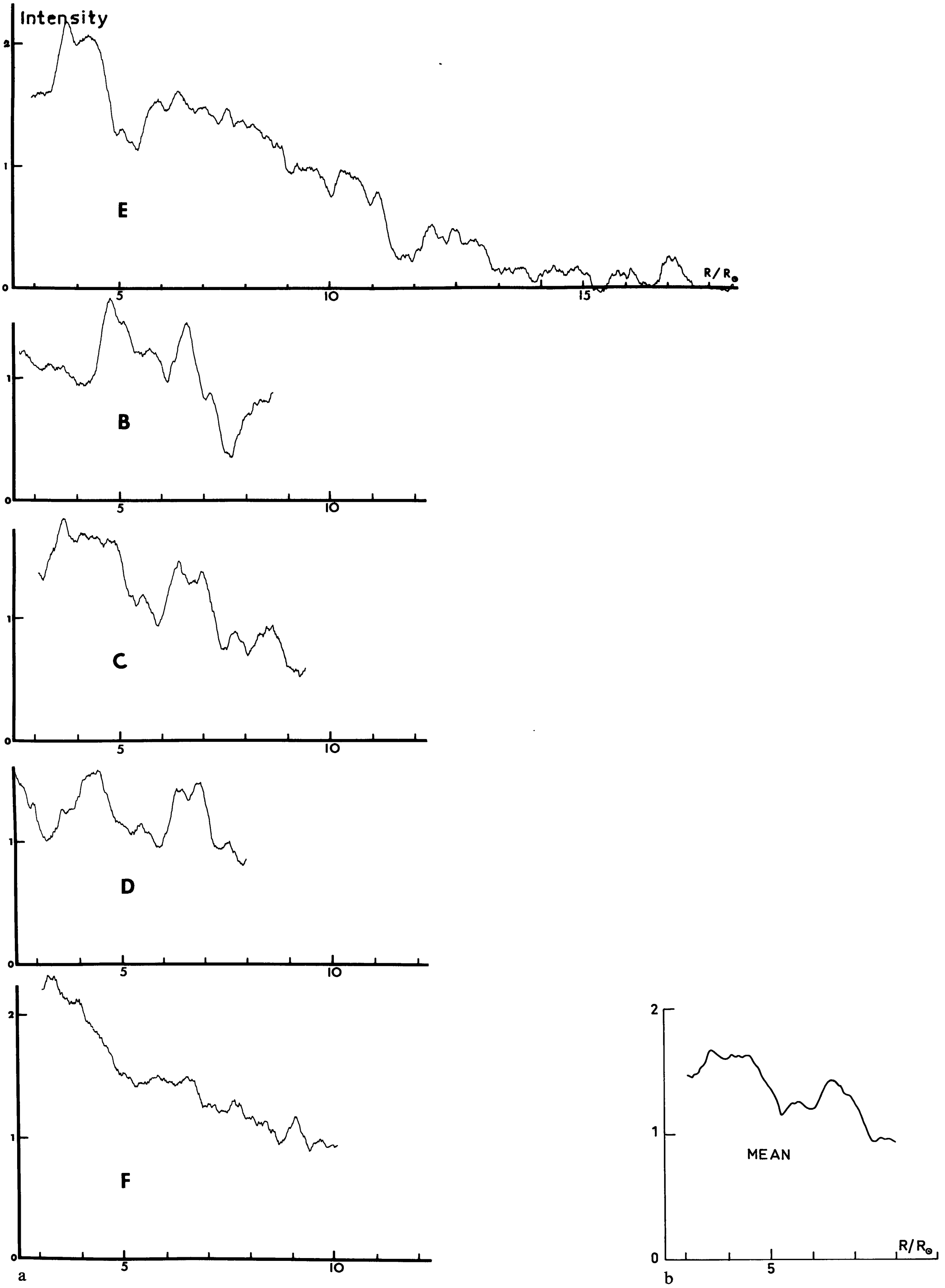

Fig. 2a and b. The differential intensity between (t) and (t′), versus solar distance $R/R_{\odot}$ along the scanning axis. Intensity units are 3.7 μW cm^{-2} $sterad^{-1}$ μ^{-1}. Scan identification refers to Table 1 nearly linear with time and zero levels for the individual scans have been determined in the following manner. Scan *E* extends to nearly 20 $R_\odot$ and although it is not proved that the features appearing beyond 15 $R_\odot$ are all real, the noise analysis indicates they are well above the instrumental noise. Therefore the minimum values of intensity beyond 15 $R_\odot$ have been used to set the baseline. The same correction has been applied to Scans *C* and *D* and Scans *B* and *F* have been zeroed to give the same intensity as Scan *E* in the characteristic region around 6.5 $R_\odot$ (the corrections in this case are $+1.4\,\mu\mathrm{W\,cm^{-2}\,sterad^{-1}}\,\mu^{-1}$ for Scan *B* and $-1.5\,\mu\mathrm{W\,cm^{-2}\,sterad^{-1}}\,\mu^{-1}$ for Scan *F*). The data was considerably over sampled when digitized during the eclipse and the scans shown in Fig. 2 have been numerically filtered by a 10 point running mean to a cut-off compatible with the 4.2 arcmin aperture and 1 arcmin/s gyro scan rate.

In order to verify the validity of assumptions regarding the confinement of emission to the plane of the ecliptic, it was intended to observe a series of scans perpendicular to it at selected heliocentric distances. This should have produced a derivative of the enhanced brightness distribution. Unfortunately the gyroheliostat scanned only a few arcminutes and did not permit an unambiguous measurement. The pronounced signal variation over this distance in Scan *Z* does, however, support the assumption that 10 μ brightness is confined to the ecliptic in approximately the same way as is the 2.2 μ brightness (MacQueen, 1968).

It is apparent from Fig. 2 that there is a definite feature at 4 $R_\odot$ and that there are several less prominent features further away from the sun, the most notable occurring around 6.4 $R_\odot$. Also evident is the absence of any significant structure beyond 10 $R_\odot$. The variations from one scan to another are above the noise level and probably reflect real spatial inhomogeneities in the emission. A mean value of Scans *B* to *F* has been computed and is also shown on Fig. 2.

The intensity scale of Fig. 2 was derived from calibration of the telescope/photometer by observation of the center of the solar disk. The final such calibration was made at essentially sea level from Las Palmas on June 29 at 1400 hrs local time. The instrument was in the eclipse configuration except that the four windows (Léna *et al.*, 1974) were stopped down from 10 cm to 1 cm to obtain the necessary signal attenuation. The detected signal under these conditions corresponds to a radiant power

$$P = A\Omega \int_{8}^{13.5} \phi_\odot(\lambda) \cdot T_a(\lambda) \cdot T_i(\lambda)\, d\lambda \qquad (1)$$

where A is the area of the telescope, Ω is the solid angle subtended on the source, $\phi_\odot(\lambda)$ is the specific intensity of the center of the solar disk in $\mathrm{W\,cm^{-2}\,sterad^{-1}}\,\mu^{-1}$, $T_a(\lambda)$ is the transmission of the instrument. $\phi_\odot(\lambda)$ is accurately known (Labs and Neckel, 1968) and $T_i(\lambda)$ has been determined in the laboratory. The principal uncertainty in this procedure is the determination of the change in $T_a(\lambda)$ from the sea level calibration to the altitude of the eclipse observations (17000 m)—due to fuel limitations it was not possible to observe the uneclipsed sun in flight on June 30. We have computed the correction using Las Palmas and flight meteorological data and published values for atmospheric absorption (Gates and Harrop, 1963). The accuracy of intensity calibration is estimated to be within a factor of 2.

Implicit in the calibration scale of Fig. 2 is the assumption of black-body emission by F-corona. Although this assumption was also used by Mankin *et al.* (1974) to calibrate the broad band intensity and allows the comparison, it may well be invalidated by a strong wavelength dependence of the opacity of the emitting region between 8 and 13 μ. We therefore reexamine this point below.

Noise Evaluation

Before flight testing of the equipment, a major uncertainty was the possibility that observation through the supersonic shock front at 10 μ would produce excess noise and severly limit the sensitivity of the observations. Figure 3 shows a comparison of in-flight and laboratory noise measurements for the system and it is apparent there is no degradation of performance. Quantitatively this implies that the shock front is not a limiting factor for 10 μ signals of the order of $0.1\,\mu\mathrm{W\,cm^{-2}\,sterad^{-1}}\,\mu^{-1}$. It also demonstrates the success of the elaborate noise rejection measures adopted for the instrument (Léna *et al.*, 1974).

It is important to consider the possibility of low frequency noise being present in the scans. Such effect could originate from time variations or spatial inhomogeneities in the temperature of the optics, particularly the window. The smoothness of Scan *E* beyond 15 $R_\odot$ and of the Scans *G–J* places an absolute

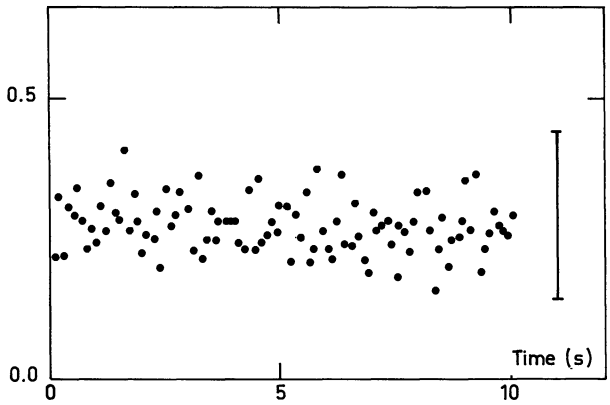

Fig. 3. An *unsmoothed* sample of the noise, recorded at the end of Scan *E*. Units are the same as on Fig. 2. Bar is the peak-to-peak noise in the laboratory for a sample of similar duration

upper limit of 0.08 μW cm^{-2} $sterad^{-1}$ μ^{-1} on such effects and they are almost certainly substantially less than this.

Spectral Observations

The second portion of totality was devoted to spectral observations. The 8–13 μ region was scanned 96 times with a filter wheel spectrometer for 6.5 min. It was intended to observe the prominent feature around 4 $R_\odot$ but field rotation and acquisition difficulties led to the spectrum being taken from the area marked by a box in Fig. 1. This was well inside the 4 $R_\odot$ feature.

The averaged spectrum is shown on Fig. 4. The zero level drift correction was established by extrapolation from Scan *I* made just before (see Table 1) and is marked by a dotted line. The bandwidth of 0.3 μ is the result of filter characteristics, response time of instrument and scanning speed. The noise level on the spectrum is simply deduced from the co-adding of individual spectral scans. The O_3 absorption correction is made on the basis of 0.26 cm STP of ozone above the mean flight altitude of 17 km. The same intensity units of Fig. 2 have been used on the intensity scale of Fig. 4, the larger values reflecting the co-adding of 96 scans; every other gain in the experiment has remained the same.

To obtain an absolute calibration in terms of monochromatic intensity, the absolute response *g* of the system has been determined both on the Sun and on a laboratory blackbody:

$$g = 4.9 \times 10^4 \text{ units/W cm}^{-2} \text{ sterad}^{-1} \mu^{-1}.$$

Knowing the spectral transmissions $T_i(\lambda)$ and $T_a(\lambda)$, and the system bandpass, one determines an absolute monochromatic flux scale: on Fig. 4, one unit corresponds to 0.7 μW cm^{-2} $sterad^{-1}$ μ^{-1}.

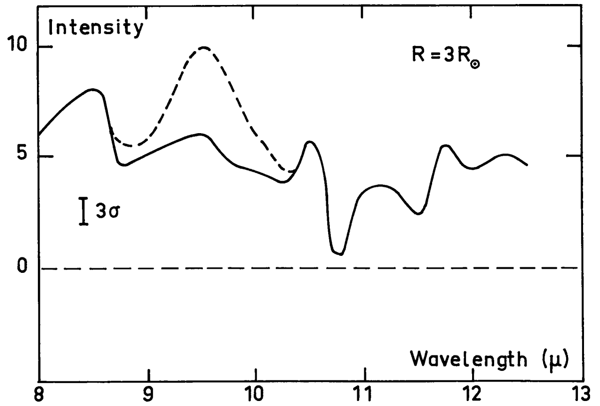

Fig. 4. Final spectrum after summation of individual spectra. Spectrum corrected from instrument transmission $T_i(\lambda)$: ———. Spectrum corrected also for atmospheric ozone absorption: – – – – –. The horizontal zero line (— — —) is the level of DC unbalance between t and t′. Monochromatic flux is 0.7 μW cm^{-2} $sterad^{-1}$ μ^{-1} per ordinate unit

Conclusions

The principal result is that F-coronal features observed at shorter infrared wavelengths are evident at 10 μ. The agreement is particularly striking for the feature at 4 $R_\odot$. The measured intensity of 7 μW cm^{-2} $sterad^{-1}$ μ^{-1} at the peak of this feature is entirely consistent with the interpretation of the feature as due to thermal emission by hot dust near the ecliptic. Moreover, this value has been computed with the blackbody assumption for dust radiation and is overestimated. On the same premises, the means intensity at 3 $R_\odot$ (Scans *B* to *F*) is 5.5 μW cm^{-1} $sterad^{-1}$ μ^{-1} but the integrated monochromatic intensity as calibrated above corresponds to a mean value over the band pass of 3.9. If the same spectrum prevails at the 4 $R_\odot$ peak, the true intensity would only be 5 μW cm^{-2} $sterad^{-1}$ μ^{-1}.

This flux value is still quite above Kaiser's (1968) prediction, and also contradicts the upper limit of Mankin *et al.* (1974), given to be 1 to 2 μW cm^{-2} $sterad^{-1}$ μ^{-1}. Kaiser's parameter on space density was set to fit the observations of MacQueen (1968) at 2.2 μ but more recent results at this wavelength by Lamy and Koutchmy (1974) tend to indicate higher values of the flux.

The spectrum shown on Fig. 4, after correction for ozone absorption, shows a complete lack of emission at 10.8 μ, which *well corresponds to the minimum emissivity wavelength of silicate-type materils*. Moreover, an emission peak is visible at 9.5 μ again in agreement with the properties of such material, as analysed for example by Lamy (1974). This author shows that andesite-type material (a rock) does not reach 3 $R_\odot$, but obsidian-type glass has a concentration and sublimation zone between 2.2 and 3.5 $R_\odot$. The emissivity rise beyond 11 μ may be attributed to quartz, as studied by Kaiser (1968). Finally, the lack of emission at 10.8 μ confirms the absence of any opaque material in significant amount at this distance from the Sun, as predicted by Lamy for iron. It may also rule out the presence of graphite (Mukai and Mukai, 1973), or of more refractory material hypothetically formed in the Sun as the oxydes collected by Hemenway *et al.* (1972).

To summarize, the present observations give the first clear indication on the existence of silicates in the interplanetary medium and confirm, at least in first approximation, the dynamics of small particles when they approach the Sun.

The observations also demonstrate that potential reductions in infrared sky noise can be achieved during observations from supersonic aircraft. The extended duration of totality afforded by the Concorde is adequate for complex observing programs. It would be of great value to repeat the multi-channel photometric observations and to obtain improved spectral and possibly polarization observations of bright F-coronal features.

Acknowledgements. The experiment was prepared in a very short period of time and its success is due to efforts by many people. We are grateful to colleagues and technical personnel at Laboratoire de Physique Stellaire et Planétaire, Centre National d'Etude de Télécommunications, Institut National d'Astronomie et de Géophysique NASA Ames, Observatoire de Meudon and Kitt Peak National Observatory. We also wish to express our appreciation of the generous support provided by the Aérospatiale and of the effort by the support team. The whole project has been supported by the Délégation Générale à la Recherche Scientifique et Technique, the Institut National d'Astronomie et de Géophysique (INAG) and the Aérospatiale.

References

Beckman, J., Bégot, J., Charvin, P., Hall, D., Léna, P., Soufflot, A., Liebenberg, D., Wraight, P. 1973, *Nature* **246**, 72
Calbert, R., Beard, D. B. 1972, *Astrophys. J.* **176**, 497
Gates, D., Harrop, W. 1963, *Appl. Optics* **2**, 887
Harwit, M. 1964, *Mem. Soc. Roy. Sc. Belgique* 5° Serie, IX, 506
Hemenway, C., Hallgren, D., Schmelberger, D. 1972, *Nature* **238**, 256
Kaiser, C. F. 1970, *Astrophys. J.* **159**, 77
Koutchmy, S. 1972, *Astron. & Astrophys.* **16**, 103
Labs, D., Neckel, H. 1968, *Z. Physik* **69**, 1
Lamy, P. L. 1974, *Astron. & Astrophys.* **33**, 191
Lamy, P., Koutchmy, S. 1974, *Astron. & Astrophys.* (submitted)
Léna, P., Viala, Y., Mondellini, J., Hall, D., McCurnin, T. W., Soufflot, A., Darpentigny, C. 1974, *Astron. & Astrophys.* **37**, 75
MacQueen, R. M. 1968, *Astrophys. J.* **154**, 1059
Mankin, W. G., MacQueen, R. M., Lee, R. H. 1974, *Astron. & Astrophys.* **31**, 17
Mukai, T., Mukai, S. 1973, *Publ. Astron. Soc. Japan* **25**, 481
Peterson, A. W. 1963, *Astrophys. J.* **138**, 1218
Peterson, A. W. 1967, *Astrophys. J.* **148**, L 37
Peterson, A. W. 1971, *Bull. Am. Astron. Soc.* **3**, 500

P. Léna
Y. Viala
Observatoire de Meudon
F-92190 Meudon, France

D. Hall
Kitt Peak National Observatory
P.O. Box 26732
Tucson, Arizona 85726, USA

A. Soufflot
Laboratoire de Physique Stellaire et Planétaire
BP 10
F-91370 Verrières le Buisson, France